Journal of Molecular Modeling (2020) 26: 328
https://doi.org/10.1007/s00894-020-04585-0

ORIGINAL PAPER

A MEDT computational study of the mechanism, reactivity and selectivity of non-polar [3+2] cycloaddition between quinazoline-3-oxide and methyl 3-methoxyacrylate

Abdelmalek Khorief Nacereddine[1]

Received: 20 July 2020 / Accepted: 22 October 2020 / Published online: 4 November 2020

Abstract

The Molecular Electron Density Theory (MEDT) was used for the study of the mechanism and the selectivity of the [3+2] cycloaddition reaction between quinazoline-3-oxide and methyl 3-methoxyacrylate, using the B3LYP/6-31G(d,p) DFT method. In gas phase, this [3+2] cycloaddition reaction is characterized by a completely *ortho* regioselectivity and a moderate *exo* stereoselectivity. Dichloroethane solvent did not modify the selectivities obtained in gas phase but increase the activation energies and decrease the exothermic character. Analysis of thermodynamic characters indicates that by the inclusion of the experimental conditions, the reaction becomes endergonic and thereby under thermodynamic control favouring the formation of the most stable product as observed experimentally, explaining the *exo* stereoselectivity. The analysis of the global electron density transfer (GEDT) at the transition states and bond order (BO) show that this reaction takes place via a very slightly synchronous and non-polar one-step mechanism. Conceptual DFT reactivity indices analysis accounts for the electrophilic character of the reagents, explaining the high obtained free activation energies, while local Parr functions analysis allows us to explain the *ortho* regioselectivity observed experimentally. ELF topological analysis of the most favoured reactive pathways indicates that mechanism of this 32CA reaction is one stage, one step, synchronous and non-concerted. The stability of the favourable cycloadduct is attributed to the presence of different non-conventional hydrogen bonds interactions as indicated by NCI and QTAIM analyses.

Keywords Mechanism · Reactivity · Selectivity · Cycloaddition · DFT calculations · MEDT

Introduction

Quinazolines are very important structures, which were found in a tremendous biological active molecules displaying a vast spectrum of pharmacological properties [1–5]. Likewise, isoxazolidines are also a very important heterocyclic molecules having a large broad potential biological and medicinal activities [6, 7].

The link of two biological active compounds is an important modern strategic synthetic technique, which is used for enhancing the primary pharmacological properties. Thereby, the link between quinazoline and isoxazolidine scaffolds produce a new type of polyheterocycle, the isoxazolo[2,3-c]quinazolines (Scheme 1), largely used in the pharmaceutical industry because of its pharmacological properties [8, 9].

Today, synthesis of complex molecules with efficient disastereo and enantioselective manner using simple substrates imposes a huge challenge in contemporary organic chemistry at industrial and academic level. To achieve those structures, [3+2] cycloaddition (32CA) reactions have been used, which are considered as a key synthetic method for the preparation of five heterocyles from simple reagents and through simple processes [10]. In this context, 32CA reaction of quinazoline-3-oxide with ethenes is a simple method for the synthesis of polyheterocyclic compounds having both quinazoline and isoxazolidines rings (Scheme 2).

Supplementary Information The online version contains supplementary material available at https://doi.org/10.1007/s00894-020-04585-0.

✉ Abdelmalek Khorief Nacereddine
a.khorief@enset-skikda.dz; malek_khorief@yahoo.com

[1] Laboratory of Physical Chemistry and Biology of Materials, Department of Physics and Chemistry, Higher Normal School of Technological Education-Skikda, Azzaba, Skikda, Algeria

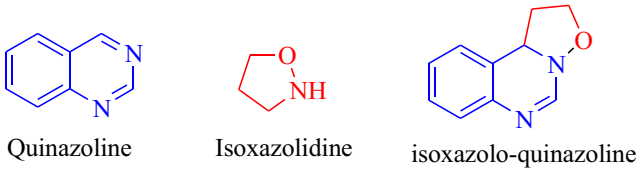

Scheme 1 Structure of quinazoline, isoxazolidine and isoxazolo[2,3-c]quinazoline

Recently, Yin and co-workers studied experimentally the 32CA of quinazoline-3-oxide (nitrone **1**) with methyl 3-methoxyacrylate (acrylate) **2** (Scheme 3). The authors have found that isoxazolo[2,3-c]quinazolines were obtained in good yield with total regio- and stereoselectivities[11].

In recent years, the most important challenge of both experimental and theoretical chemists is predicting the reactivity and selectivity of molecules before and during the reaction. In order to understand, interpret and predict the mechanistic behaviours of organic reactions, many theoretical models have been proposed, such as Houk's FMO model based on the interaction between frontier molecular orbitals [12] and the recent Domingo's theory, the Molecular Electron Density Theory (MEDT) [13], which is based on the change of electron density during the reaction.

The main objective of our research axis is to predict the molecular mechanism and understanding the origin of the selectivity of the cycloaddition reactions for the synthesis of active complex biological compounds [14–19]. Herein, we focused on a MEDT study of the 32CA reactions, with the aim of comprehending the factors controlling the regio- and stereoselectivities of the 32CA reaction performed by Yin's group [11].

Computational methods

The structures of stationary points were optimized using the hybrid functional B3LYP and the 6-31G (d,p) basis set [20–23] within the program Gaussian 09 [24]. The nature of all stationary points has been confirmed by frequency calculations, in which reagents and products do not present any imaginary frequency, while transition states (TSs) must have one and only one imaginary frequency. The electronic structure of the transition states were analysed using NBO method [25]. The effect of the solvation of dichloroethane (DCE) was performed using the polarisable continuum model (PCM) [26] through the self-consistent reaction field (SCRF) [27–29]

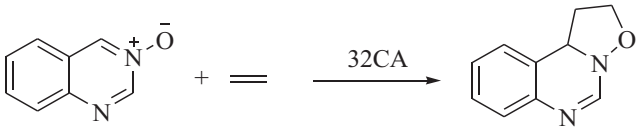

Scheme 2 Synthesis of isoxazolo-quinazoline by 32CA of quinazoline-3-oxide and ethylene

within single point calculations of the optimized gas phase structures. Values of thermodynamic properties, namely, Gibbs free energies, enthalpies and entropies, were calculated at 333 K and 1 atm through the optimized gas phase structures [30]. The electrophilic index ω [31] is given by the equation, $\omega = (\mu^2/2\eta)$. The electronic chemical potential μ and the hardness η were calculated according to the following formulas: $\mu = (\varepsilon_{HOMO} + \varepsilon_{LUMO})/2$ and $\eta = \varepsilon_{LUMO} - \varepsilon_{HOMO}$, in which ε_{HOMO} and ε_{LUMO} are the energies of the frontier molecular orbitals, respectively [32, 33]. The P_K^+ electrophilic and P_K^- nucleophilic Parr functions [34] which are used for obtaining the electrophilic and nucleophilic centres of the separated reagents were calculated using the Mulliken atomic spin density (ASD) of the radical anion and the radical cation of the electrophile and the nucleophile, respectively.

Non-covalent interaction (NCI) analysis was performed within the reduced density gradient and low-gradient isosurfaces [35, 36], using NCI plot [37]. Quantum theory of atoms in molecule (QTAIM) [38] was performed using the Multiwfn [39] program, through the corresponding B3LYP/6-31G(d,p) mono-determinantal wave function.

The global electron density transfer (GEDT) [40] was calculated of the sum of the natural atomic charges obtained by a natural population analysis (NPA) of the atoms constructing the reagents [41]. Electron localization function (ELF) [42] topological analysis was realized using the Multiwfn [39] program through the corresponding B3LYP/6-31G(d) mono-determinantal wave function.

Results and discussion

In this part, firstly, we analyse the energy profiles of all possible reactive pathways corresponding to this 32CA reaction. We also analyse the geometries of the transition states and GEDT which occurred at the transition states. Secondly, we study the reactivity and the regioselectivity of this 32CA reaction using conceptual DFT (CDFT) reactivity indices [43, 44] and local Parr functions indices [34], respectively. In the third part of this study, we study the electronic structure of the different molecular systems at the most favourable profile in terms of ELF analyses in order to predict the molecular mechanism nature of the studied 32CA reaction. Finally, the *ortho-exo* selectivity of the present 32CA reaction is analysed in terms of NCI and QTAIM analyses techniques.

Energy and geometry analysis

Because the reagents nitrone **1** and acrylate **2** have an asymmetric structure, the 32CA reaction between them can follow four possible reactive pathways, namely, the *ortho* and *meta* regioisomeric channels, and in each regioisomeric channel,

Scheme 3 Experimental [3+2] cycloaddition between nitrone **1** and acrylate **2**

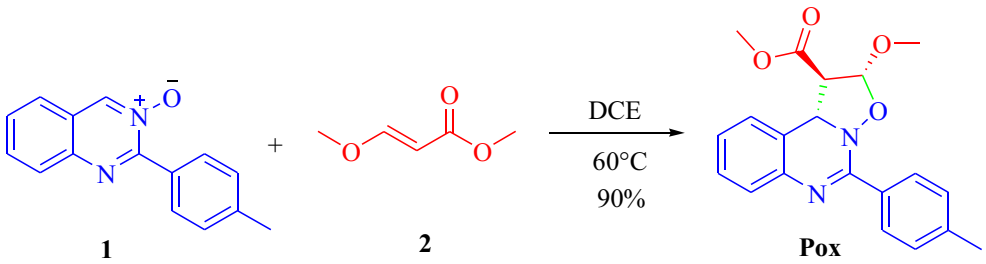

the regents may approach one to the other through two possible stereoisomeric pathways, that are the *endo* and *exo* approaches. So, in addition to the separated reagents nitrone **1** and acrylate **2**, in the studied 32CA reaction, four possible transition states, **TSon**, **TSox**, **TSmn** and **TSmx**, and four possible cycloadducts **Pon**, **Pox**, **Pmn** and **Pmx**, may be formed which have been located and characterized (Scheme 4). The calculated total energies in gas phase and in dichloroethane (DCE) solvent of the stationery points are given in Table S1 in the Supporting Information, while the corresponding relative ones are given in Scheme 4. The Cartesian coordinates of the stationary points and the imaginary frequencies of the transition states are included in the Supporting Information.

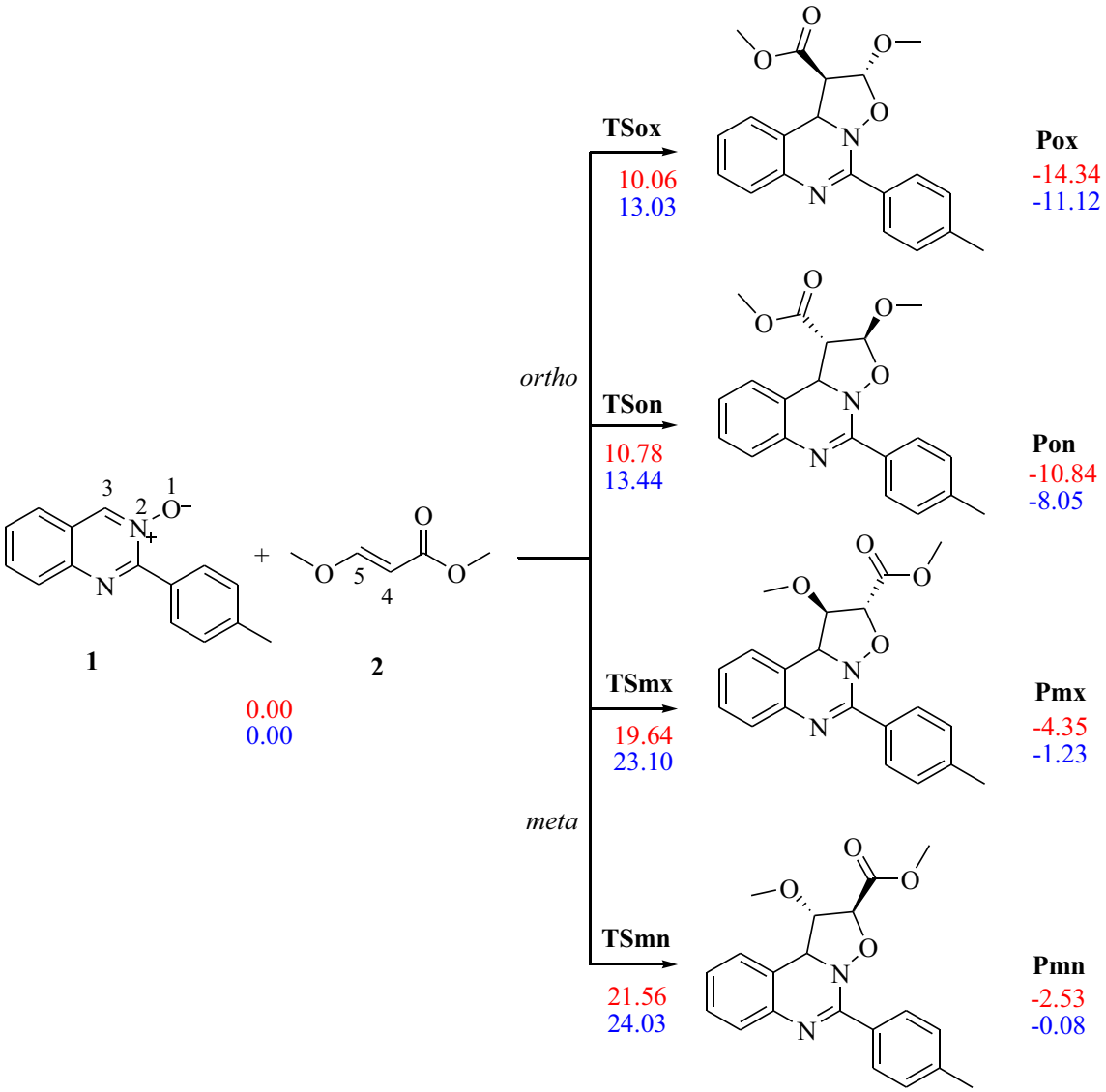

Scheme 4 The pathways involved in the [3+2] cycloaddition reaction of nitrone **1** with acrylate **2** together with relative energies, red in gas phase and blue in solution

From the values of activation energies in the gas phase, the noticeable remark is that a small activation energy difference between that of the *ortho* pathways (0.72 kcal mol^{-1}), thereby, this 32CA reaction can lead kinetically to the formation of a mixture of both **Pmn** and **Pmx**, in which this last is slightly kinetically favoured. In addition, we notice that the *meta* cycloadducts are less stable, indicating that these pathways are unfavourable both kinetically and thermodynamically. Therefore, this 32CA reaction is completely *ortho* regioselective, as observed experimentally.

Because the gas phase does not reproduce all experimental outcomes, in particular, total stereoselectivity, further calculations taking into account experimental conditions such as solvent nature are necessary. From the values of relative energies of TSs and CAs in the solution phase, we notice that there is an increase of activation energies by about 3 kcal mol^{-1} and a decrease of the exothermic character of these pathways in comparison to the gas phase values. This fact may be due to the better solvation of the reagents than the TSs and CAs [45], because the reagents are more polarized than TSs and/or cycloadducts, which favour the formation of a strong electrostatic interactions with solvent molecules.

Since this 32CA between nitrone **1** and acrylate **2** is under thermodynamic control, and the non-covalent interactions at the most stable cycloadduct (**Pox**) are governed by the selectivity (see "Origin of the stability of Pox" section), further calculations including diffuse functions may be more suitable and reliable for the study of these molecular systems. Thereby, we have performed single point calculations at B3LYP/6-31+g(d,p)//B3LYP/6-31G(d) level of theory. The energy results are given in Table 1.

From Table 1, the difference in relative energy between that of the most stable cycloadduct (Pox) and the second one (**Pon**) is 3.37 kcal mol^{-1}. This value is almost the same obtained using the standard 6-31G(d) basis set (3.53). Therefore, the inclusion of diffuse functions in calculations does not make any remarkable change in the selectivity. Consequently, the B3LYP/6-31G(d) level is appropriate for the study of this systems despite the existence of non-covalent interactions.

The solution activation energies difference ($\Delta\Delta E$ = 0.41 kcal mol^{-1}) is small and thereby does not reproduce the stereoselectivity observed experimentally; therefore, we are obliged to include in calculations other experimental conditions such as temperature, which was 60 °C and pressure (1 atm) and solvent nature (DCE). From the obtained results, we can extract the thermodynamic properties, namely, enthalpy, entropy and free energy. The values of the relative thermodynamic parameters are collected in Table 2, while the total ones are moved to Table S2 in the Supporting Information. The free energy profiles for the four completive pathways are depicted in Fig. 1.

By taking into account the thermal parameters in calculation, the previous obtained *ortho* regioselectivity obtained experimentally and in the previous calculations does not change, in which the activation enthalpy difference between the *ortho* paths is $\Delta\Delta H = 0.40$ kcal mol^{-1}. Furthermore, the positive sign of relative enthalpies of the *meta* cycloadducts indicates that the corresponding pathways become having an endothermic character, stressing in addition its unfavourable formation. On the other hand, the values of activation free energies increase by about 15 kcal mol^{-1} in compared to the obtained activation enthalpies. This increase may be explained by the negative values of the corresponding entropy which is consequence of the bimolecular character of this 32CA reaction. Besides, the positive values of relative free energies account that all competitive pathways become having an endergonic character. Thereby, the studied 32CA reaction is under thermodynamic character, in which the more stable cycloadduct is thermodynamically the more favoured product. Consequently, the **Pmx** (8.19 kcal mol^{-1}) is the favoured thermodynamic product since it is 2.18 kcal mol^{-1} more stable

Table 1 B3LYP/6-31+g(d,p)//B3LYP /6-31G(d,p) total and relative energies, in gas phase of the stationery points involved in the 32 CA reaction of nitrone **1**with acrylate **2**

System	E (a.u)	ΔE (kcal mol^{-1})
Nitrone 1	− 763.551782	
Acrylate 2	− 421.024744	
TSox	− 1184.55438	13.90
TSon	− 1184.55437	13.90
TSmx	− 1184.53653	25.10
TSmn	− 1184.53878	23.69
Pox	− 1184.59224	− 9.86
Pon	− 1184.58687	− 6.49
Pmx	− 1184.57395	1.62
Pmn	− 1184.57666	− 0.08

Table 2 Relative enthalpies, entropies and Gibbs free energies for the TSs and the cycloadducts involved in the 32CA between nitrone **1** and acrylate **2**

System	ΔH (kcal mol^{-1})	ΔS (cal mol^{-1} K^{-1})	ΔG (kcal mol^{-1})
TSox	13.83	− 48.267	29.91
TSon	14.23	− 46.663	29.78
TSmn	24.63	− 49.327	41.06
TSmx	23.64	− 49.699	40.19
Pox	− 8.49	− 50.071	8.19
Pon	− 5.59	− 47.921	10.37
Pmn	2.28	− 48.92	18.57
Pmx	1.15	− 49.231	17.55

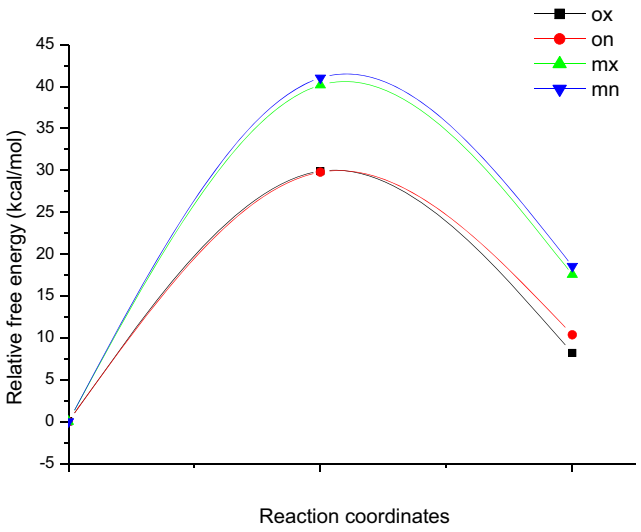

Fig. 1 Relative Gibbs free energy profile of the pathways associated with the 32CA reaction of nitrone **1** with acrylate **2**

than the second more stable one **Pmn** cycloadduct (10.37 kcal mol^{-1}). Resulting from that, this 32CA reaction leads to the formation of only a single regio- and steroisomer as the kinetic and thermodynamic cycloadduct which is **Pmx**, in great accordance with experimental data [11].

On the other hand, the used experimental thermal condition of this 32CA reaction (60 °C) is explained by these relatively high values of free energies.

The optimized structures of the transition states of the 32CA reaction between nitrone **1** and acrylate **2** as well as the lengths of the new forming bonds, the corresponding bond order, the values and direction of GEDT are given in Fig. 2.

The analysis of the synchronicity of mechanism was performed on the basis of Wiberg bond indices [46]. The bond order (BO) values at the TS indicates that the formation progress of new forming bonds C–C and O–C is 37% and 0.41% at **TSox**, 37% and 41% at **TSon**, 50% and 36% at **TSmx** and 50% and 41% at **TSmn**. These values indicate that the mechanism is almost asynchronous in all paths, in which, in the *ortho* pathways, the formation of the C–O new bond is slightly advanced than that of the C–C one and vice versa in the *meta* ones.

We have obtained a negative sign of GEDT, which was calculated from the nitrone **2** system at transition states; therefore, the flux of the electron density unfolds from acrylate **2** to nitrone **1**. The obtained very low values accounting for a non-polar character for these 32CA reactions and explaining the obtained high activation Gibbs free energies.

Analysis of the conceptual DFT indices at the ground state of the reagents

Table 3 contains the energies of frontier molecular orbitals (FMO) and values of global CDFT reactivity indices of nitrone **1** and acrylate **2**.

For the electronic chemical potential values and by a comparison between that of both reagents, acrylate **2** (− 3.59 eV) and nitrone **1**, (− 3.88 eV), the flux of electronic density named as GEDT which occur at the transition states will take place from acrylate **2** system to the nitrone **1** one. For the electrophilic indices values, nitrone **1** has 2.01 eV and acrylate **2** possesses 1.12 eV, accounting that nitrone **1** is a strong electrophile, while acrylate **2** in the borderline between strong and moderate electrophile based on the electrophilic scale proposed by Domingo et al. [47]. Therefore, this 32CA reaction occurred between two reagents with almost the same electronic behaviours, which explain the high free activation energy and the low values of GEDT.

Figure 3 presents a three-dimensional illustration of the atomic spin densities (ASD) of the radical cation nitrone $\mathbf{1}^{\cdot}$, and the radical anion acrylate $\mathbf{2}^{+}$, as well as the nucleophilic Parr functions local indices of acrylate **2** and the electrophilic Parr functions local indices of nitrone **1**. From Fig. 3, the higher electrophilic P_K^+ Parr function local index is concentrated at the carbon atom C3 as can be seen at the reactive region of the nitrone **1** (for atom numbering, see Scheme 4), with a value of $P_K^+ = 0.26$. In contrast, for the nucleophilic P_K^- Parr function local indices of acrylate **2**, we can clearly see at the C4=C5 reactive region that C4 has the higher value of local indices ($P_K^- = 0.54$), which reveals that it is the most nucleophilic centre in this nucleophilic reagent. Based on the fact that in polar mechanisms, the favourable interaction between reactive centres will be of the most electrophilic centre of the electrophile with the most nucleophilic centre of the nucleophile [47], the present 32CA reaction will form only the *ortho* regioisomers. This finding is in agreement with the analysis of energy profiles and explains well the experimental data [11].

ELF analysis (nature of molecular mechanism)

We have planned to investigate the electronic nature of the molecular mechanism for the most favoured reactive path associated to the 32CA reaction between nitrone **1** and acrylate **2** in order to get more detailed characterization of the changes in the electronic density during the studied 32CA reaction. For achieving this goal, we have performed an electron localisation function (ELF) topological analysis of pertinent selected points on the IRC curve associated with the formation of Pox. The IRC profile of the *ortho-exo* path together with the selected pertinent points, from **MC** to **Pox** associated to this pathway, are displayed in Fig 4. The electronic populations of the most important ELF valence basins of the selected structures are collected in Table 4. The ELF attractor positions of the selected structures on the IRC curve of the *ortho-exo* reactive pathway associated with the 32CA reaction of nitrone **1**

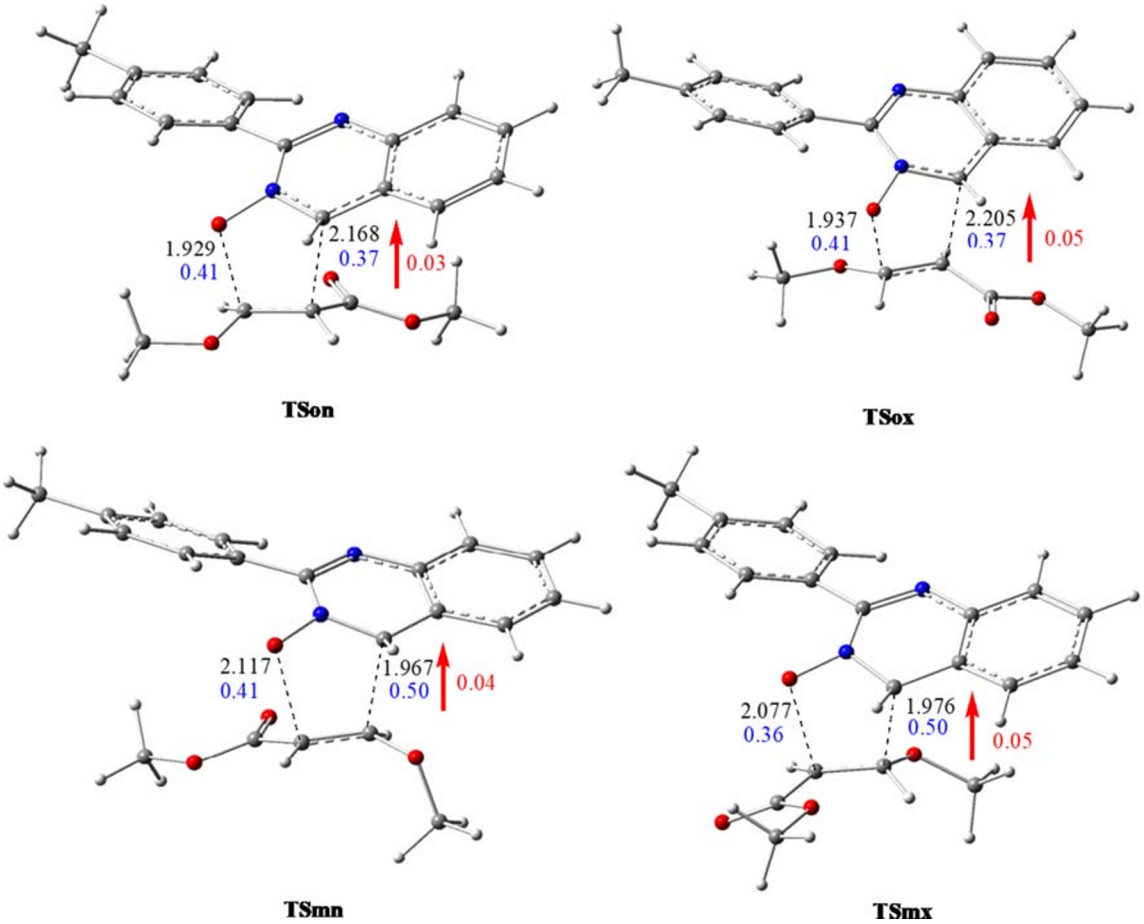

Fig. 2 Optimized geometries of the transition states involved in the 32CA reaction of nitrone **1** with acrylate **2**, together with lengths of new forming bonds (black), Wiberg indices (blue) and GEDT values (red)

with acrylate **2** together with the population of some relevant basins are depicted in Fig 5.

The most important basins are concentrated at the reactive region, the (C3−N2 and N2−O1) bonds of nitrone **1** and C4 −C5 bond of acrylate **2**.

First, the reaction began by a rapprochement of reagents forming a molecular complex (**MC**), which stabilizes by electrostatic interactions. Thereby, the **MC** ELF topological structure shows the presence of a V(C4,C5) and V'(C4,C5) disynaptic basins which are characterized by a population of 3.52e for each one, accounting for a high electron density of this reactive region, in great agreement with the global reactivity indices, which is classified as a nucleophile species. This is due to the electron-donating group (methoxy) that is conjugated with the C=C double bond of the acrylate. On the other hand, the N2−O1 bond shows the presence of V(N2,O1) disynaptic basin with a population of 1.28e. In addition, we notice that the presence of V(C3,N2) disynaptic basin integrating 3.28e.

Table 3 FMO energies and global CDFT indices, in eV, of nitrone **1** and acrylate **2**

	HOMO	LU MO	μ	η	ω
Nitrone 1	− 5.76	− 2.01	− 3.88	3.75	2.01
Acrylate 2	− 6.48	− 0.71	− 3.59	5.77	1.12

The second selected point is **P1**, just before the transition state. The remarkable change at this point is the apparition of two new monosynaptic V(N2) and V(C4) basins with a population of 0.94 and 0.42e, respectively. The monosynaptic V(N2) accounts for the beginning of the formation of N nonbonding electron pair which is formed from the decrease of the electron density of the V(C3,N2) disynaptic basin which becomes integrating 2.41e. The monosynaptic V(C4) accounts also for the beginning of the formation of pseudoradical centre at C4 atom from the decrease of electron density of the C4−C5 reactive region, which may be noticed by the disappearance of a V'(C4,C5) disynaptic basin and decreases of electron density of V(C4,C5) disynaptic basin by 0.60e.

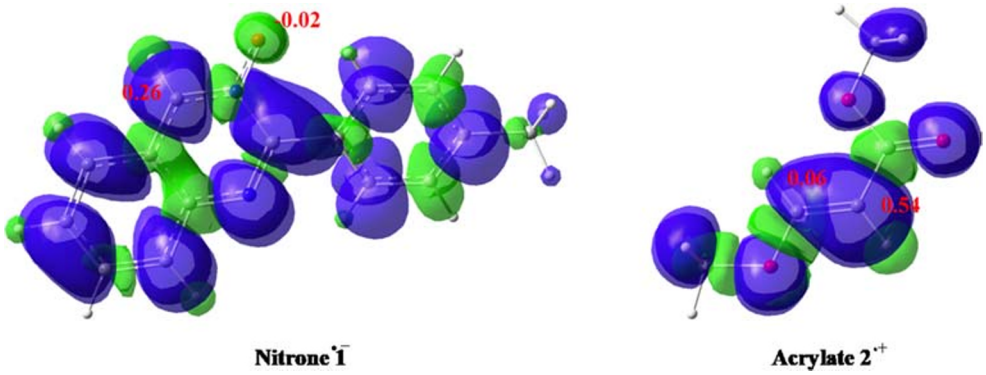

Fig. 3 Illustration of ASD associated with the radical cation $\mathbf{1}^{\bullet-}$, and the radical anion $\mathbf{2}^{\bullet+}$, together with the nucleophilic Parr functions local indices of acrylate **2** and the electrophilic Parr functions local indices of nitrone **1**

At the transition state **TSox**, where, d(C3−C4) = 2.20 Å and d(O1−C5) = 1.93 Å, the noticeable change is the apparition of new V(C3) monosynaptic basin with a population of 0.34e, accounting for the formation of a pseudoradical C3 centre. In addition, the V(N2−C3), V(C4,C5) and V(N2-O1) disynaptic basins continue to be depopulated and the electronic population of V(C4) and V(N2) slightly increases.

At the first point after **TSox**, which is **P2**, where the lengths of the new forming bonds, C3−C4 and O1−C5 are 2.06 Å and 1.79 Å, respectively. At this point, in addition to the depopulation of the disynaptic basins of the reactive regions and the population of the new monosynaptic basins, the main topological change is the apparition of new monosynaptic V(C5) basin with a population of 0.26e.

The most important point is **P3**, because here, we can notice the vanishment of the V(C3), V(C4) and V(C5) monosynaptic basins and a formation of new V(C3,C4) and V(O1,C5) disynaptic basins characterized by 1.66 and 0.92e of electronic population, respectively, accounting for the simultaneously formation of the new single C3−C4 and O1−C5 bonds.

Finally, we noticed at cycloadduct **Pox**, where d(C3–C4) = 1.58 Å and d(O1–C5) = 1.45 Å, an increases of the population of the new V(O1,C5) and V(C3,C4) disynaptic basins which become 1.81 and 1.65e, respectively. In contrast, the electronic population of V(N2) monosynaptic basin achieve 2.08e indicates that the full formation of *N* atom nonbonding electron pair.

We extract from all of the above analyses that this 32CA reaction occurs via a one-stage one-step synchronous mechanism. Additionally, in the first place, this 32CA reaction began by the formation of non-stable pseudo-diradical centres then followed by their coupling leading to the formation of the new single bonds, and thereby, the molecular mechanism is non-concerted.

Table 4 Electronic populations of valence basin taken from ELF calculations of the selected systems corresponding to the *ortho-exo* pathway of the 32CA reaction of nitrone **1** with acrylate **2**

	MC	P1	TSox	P2	P3	Pox
d(C3−C4)	3.16	2.35	2.20	2.06	1.74	1.58
d(O1−C5)	3.84	2.09	1.93	1.79	1.53	1.45
V(N2−C3)	3.28	2.41	2.20	2.05	1.80	1.76
V(O1−N2)	1.28	1.17	1.09	1.27	1.12	0.99
V(C4−C5)	3.52, 3.52	2.92	2.74	2.33	2.12	2.00
V(C3−C4)	–	–	–	–	1.66	1.81
V(O1−C5)	–	–	–	–	0.92	1.65
V(C3)	–	–	0.34	0.50	–	–
V(N2)	–	0.94	1.22	1.49	1.88	2.08
V(C4)	–	0.42	0.59	0.74	–	–
V(C5)	–	–	–	0.26	–	–

Origin of the stability of Pox

Since this 32CA reaction is under thermodynamic control, the most stable cycloadduct **Pox** may have some non-covalent interactions more than other cycloadducts that stabilized it. Thereby, we have performed a NCI as well as QTAIM analyses in order to confirm the presence and to determine the nature of these interactions at **Pox** structure and the comparison with that of the second most stable cycloadduct **Pon**.

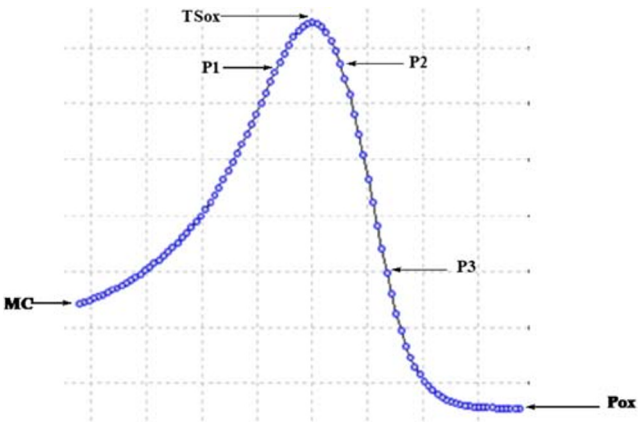

Fig. 4 The IRC profile of the favourable *ortho-exo* approach together with the positions of the selected points of the 32CA reaction between nitrone **1** and acrylate **2**

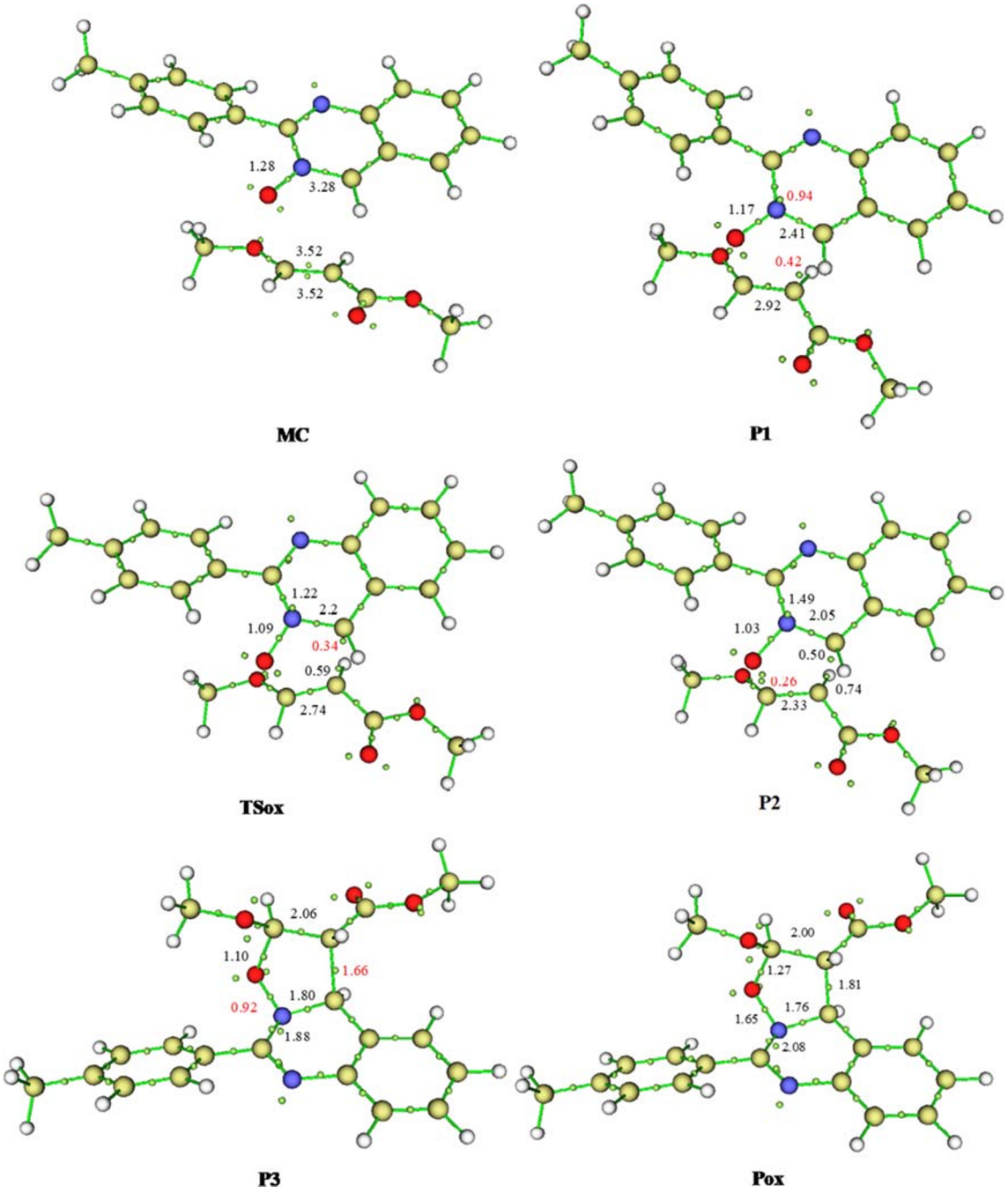

Fig. 5 Positions of ELF attractors of the selected structures on the IRC curve corresponding to the *ortho-exo* reactive pathway of the 32CA reaction of nitrone **1** with acrylate **2** together with the population of the most relevant basins

NCI analysis

Non-covalent interactions (NCI) may play an important role for the determination of the stereoselectivity of many reactions, namely, the 32CA reactions as confirmed by previous studies [48–51]. For confirming the presence of this kind of interactions, we have performed a NCI analysis of the structure of the favourable cycloadduct: **Pox** and the second one **Pon**. A preliminary analysis of the structures of both cycloadducts reveals that there are some non-covalent interactions such as C…H, N…H and O…H interactions. Therefore, these non-conventional hydrogen bonds (HB) may be enhancing the stability of these structures. For obtaining more detail about those interactions, we have

performed an NCI analysis of both structure of **Pox** and **Pon**. The reduced density gradient for **Pox** and **Pon** are depicted in Fig. 6.

Figure 6 shows the presence of several surfaces with turquoise and green colours is both Pox and Pon structures, which indicates for the presence of several weak non-covalent interactions in **Pox** and **Pon** systems.

For the sake to confirm the presence of these non-covalent interactions, a supplementary deep analysis such as QTAIM to distinguish between these them is necessary.

QTAIM analysis

Quantum theory of atom in molecule (QTAIM) analysis of the electron density in molecular system leads to different critical points (cps), in which, the (3,−1) bcp is the most important. The existence of (3,−1) bcp is associated by the presence of a stabilization interaction, namely, the hydrogen bond (HB) [52, 53]. The HB interactions may be classified into three types, [52], the strong HBs are characterized by a Laplacian, $\nabla^2\rho_{bcp} < 0$ and a total electron energy density, $H_{bcp} < 0$. A medium strength HBs are characterized by a, $\nabla^2\rho_{bcp} < 0$ and $H_{bcp} > 0$, while a weak strength HBs are defined by, $\nabla^2\rho_{bcp} > 0$ and $H_{bcp} > 0$.

As the studied 32CA reaction between nitrone 1 and acrylate 2 is under thermodynamic control, the QTAIM topological analysis [38] is performed at **Pox** and **Pon**. Thus, the QTAIM characterizing parameters of the (3,-1) critical points of **Pox** and **Pon** are collected in Table 5. The representation of the QTAIM molecular graphs of both cycloadducts is illustrated in Fig. 7.

From Fig. 7, we notice that **Pox** presents three types of stabilized non-covalent interaction which are one C…H and two O…H types. On the other hand, **Pon** presents only one O…H type interaction. Consequently, the presence of stabilized non-covalent interactions in **Pox** higher than that in **Pon** explains that **Pox** is more stable than **Pon**.

Table 5 QTAIM parameters (in a.u) of the (3,-1) bond critical points presented in **Pox** and **Pon**

Cycloadduct	BCP	Type	ρ_{cbcp}	$\nabla^2\rho_{bcp}$	H_{bcp}
	1	C…H	0.74	0.139	0.747
Pox	2	O… H	0.13	0.545	0.203
	3	O… H	0.48	0.187	0.987
Pon	4	O… H	0.13	0.556	0.223

From Table 4, we can notice that all bcps are characterized by a positive sign of Laplacian $\nabla^2\rho_{bcp} > 0$ and $H_{bcp} > 0$ of (3,-1) bcp indicate that all these interactions are weak stabilized non-conventional HBs of type C − H and O − H.

In addition, an analysis of the Laplacian of the four bcps indicates that the non-conventional H…O HB number 2 in **Pox** and number 4 in **Pon** are the strong non-covalent interactions which have the small H_{bcp} in comparison with the other bcps, but that of **Pox** is slightly more stronger.

On the other hand, the presence of two supplementary non-conventional stabilized HB, C…H and O…H, which are characterized by Laplacian $\nabla^2\rho_{bcp} > 0$ and $H_{bcp} > 0$ in **Pox** enhance its stability in comparison to **Pon** cycloadduct. Consequently, in addition to the relatively strong O…H HB in **Pox**, the presence of other two non-conventional weak interactions participate in its stabilization and thereby enhance the its favouring as a thermodynamic product of the 32CA reaction between nitrone **1**and acrylate **2**.

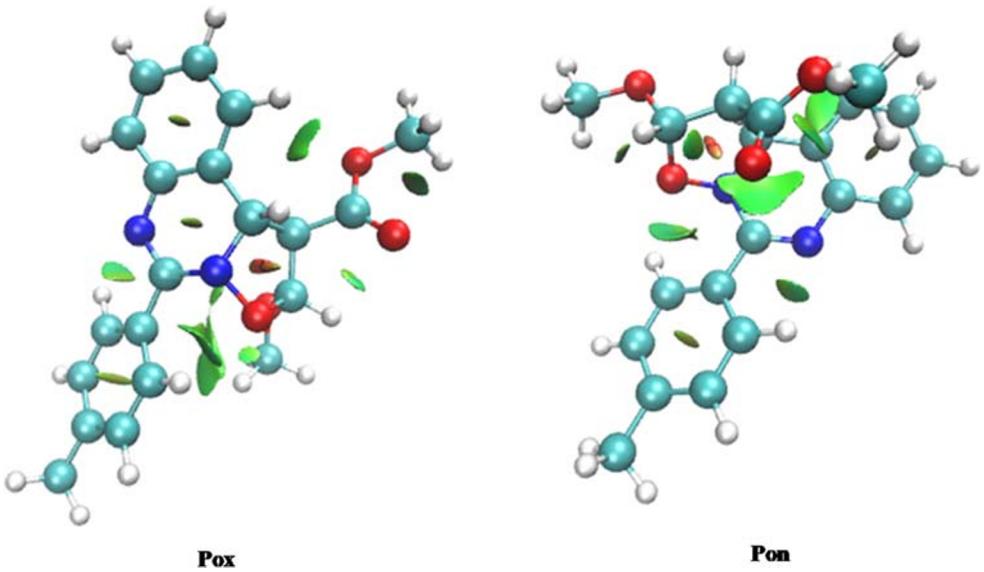

Fig. 6 NCI gradient isosurfaces of **Pox** and **Pon**

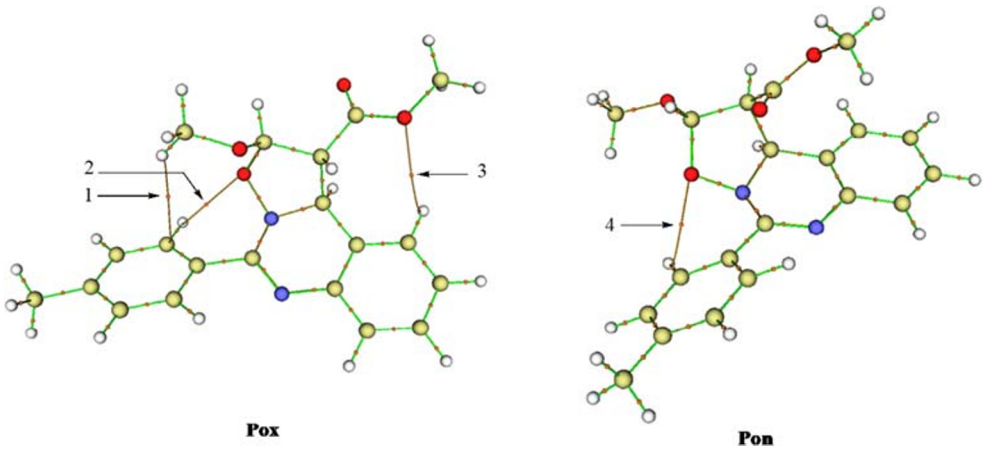

Fig. 7 Molecular graphs of **Pox** and **Pon** obtained by QTAIM analysis of electron density with (3,-1) critical points

Conclusions

The MEDT was used in this computational work for performing a deep study on the mechanism and selectivity of the 32CA reaction of quinazoline-3-oxide (nitrone **1**) with methyl 3-methoxyacrylate (acrylate) **2** within the B3LYP/6-31G(d) DFT method. The main conclusions of this work are as follows:

a Energy profile analysis in gas phase as well as in DCE solvent indicates that this 32CA reaction between nitrone **1** and acrylate **2** is under kinetic control which is completely *ortho* regioselective and moderately *exo* stereoselective, in which DCE solvent increases the activation energies and decreases the exothermic character because it stabilizes the reactants than transition states and cycloadducts.

b The IRC, bond order and GEDT analyses show that this 32CA reaction proceeds through a non-polar synchronous one step molecular mechanism.

c Inclusion of experimental conditions in calculations indicates that the studied 32CA reaction is under thermodynamic control favouring completely the formation of the *ortho-exo* cycloadduct, in greet accordance with experimental finding.

d CDFT global reactivity indices analysis indicates that both reagents have a similitude electronic behaviour explaining well the obtained high activation energy, while the experimentally *ortho* regioselectivity is interpreted in terms of local Parr reactivity indices.

e The stability of **Pox** is related presence of three non-conventional hydrogen bonds which confirmed by NCI and QTAIM analyses.

References

1. Gatadi S, Gour J, Shukla M, Kaul G, Das S, Dasgupta A, Malasala S, Borra RS (2018) Synthesis of 1, 2, 3-triazole linked 4 (3H)-quinazolinones as potent antibacterial agents against multidrug-resistant Staphylococcus aureus. Eur J Med Chem 157:1056–1067
2. Fan ZJ, Shi J, Bao XP (2018) Synthesis and antimicrobial evaluation of novel 1, 2, 4-triazole thioether derivatives bearing a quinazoline moiety. Mol Divers 22:657–667
3. Kapil S, Singh PK, Silakari O (2018) *An update on small molecule strategies targeting leishmaniasis*. Eur J Med Chem 157:339–367
4. Rahman MU, Rathore A, Siddiqui AA, Parveen G, Yar MS (2014) Synthesis and characterization of quinazoline derivatives: search for hybrid molecule as diuretic and antihypertensive agents. J Enzym Inhib Med Chem 29:733–743
5. Ugale VG, Bari SB (2014) Quinazolines: new horizons in anticonvulsant therapy. Eur J Med Chem 80:447–501
6. Patterson W, Cheung PS, Ernest MJ (1992) *3-Carboxy-5-methyl-N-[4-(trifluoromethyl) phenyl]-4-isoxazolecarboxamide, new prodrug for the antiarthritic agent 2-cyano-3-hydroxy-N-[4-(trifluoromethyl) phenyl]-2-butenamide*. J Med Chem 35:507
7. Wagner E, Becan L, Nowakowska E (2004) *Synthesis and pharmacological assessment of derivatives of isoxazolo [4, 5-d] pyrimidine*. Bioorg Med Chem 12:265
8. Carrieri A, Muraglia M, Corbo F, Pacifico C (2009) *2D-and 3D-QSAR of Tocainide and Mexiletine analogues acting as Nav1. 4 channel blockers*. Eur J Med Chem 44:1477
9. Gabrielsen M, Kurczab R, Siwek A, Wolak M, Ravna AW, Kristiansen K, Kufareva I, Abagyan R, Nowak G, Chilmonczyk Z, Sylte I, Bojarski AJ (2014) *Identification of novel serotonin transporter compounds by virtual screening*. J Chem Inf Model 54:933
10. Padwa A (ed) (1984) 1,3-Dipolar Cycloaddition Chemistry, vols. 1 and 2. Wiley/Interscience, New York
11. Yin Z, Li X, Deng Z, Yang Q, Peng Y (2020) *The synthesis of isoxazolo [2, 3-c] quinazolines via a cycloaddition of quinazoline-3-oxides and acrylates*. Tetrahedron Lett 61:151818
12. Houk KN (1975) Frontier molecular orbital theory of cycloaddition reactions. Acc Chem Res 8(11):361–369
13. Domingo LR (2016) *Molecular electron density theory: a modern view of reactivity in organic chemistry*. Molecules 21:1319–1334
14. Sobhi C, Khorief Nacereddine A, Djerourou A, Ríos-Gutiérrez M, Domingo LR (2017) *A DFT study of the mechanism and selectivities of the [3+ 2] cycloaddition reaction between 3-(benzylideneamino) oxindole and trans-β-nitrostyrene. J Phys Org Chem 30*(6):e3637
15. Nasri L, Ríos-Gutiérrez M, Nacereddine AK, Djerourou A, Domingo LR (2017) *A molecular electron density theory study of [3+ 2] cycloaddition reactions of chiral azomethine ylides with β-nitrostyrene. Theor Chem Accounts 136*(9):104

16. Ríos-Gutiérrez M, Nasri L, Khorief Nacereddine A, Djerourou A, Domingo LR (2018) *A molecular electron density theory study of the [3+ 2] cycloaddition reaction between an azomethine imine and electron deficient ethylenes*. *J Phys Org Chem 31*(6):e3830
17. Yahia W, Khorief Nacereddine A, Liacha M, Djerourou A (2018) *A quantum-chemical DFT study of the mechanism and regioselectivity of the 1, 3-dipolar cycloaddition reaction of nitrile oxide with electron-rich ethylenes*. *Int J Quantum Chem 118*(11):e25540
18. Barama L, Bayoud B, Chafaa F, Nacereddine AK, Djerourou A (2018) *A mechanistic MEDT study of the competitive catalysed [4+ 2] and [2+ 2] cycloaddition reactions between 1-methyl-1-phenylallene and methyl acrylate:* the role of Lewis acid on the mechanism and selectivity. Struct Chem 29(6):1709–1721
19. Chafaa F, Nacereddine AK, Djerourou A (2019) *Unravelling the mechanism and the origin of the selectivity of the [3+ 2] cycloaddition reaction between electrophilic nitrone and nucleophilic alkene*. *Theor Chem Accounts 138*(12):123
20. Lee C, Yang W, Parr RG (1988) *Development of the Colle-Salvetti conelation energy formula into a functional of the electron density*. Phys Rev B 37:785
21. Becke AD (1993) Density-functional thermochemistry. I. The effect of the exchange-only gradient correction. J Chem Phys 98:5648
22. Hehre WJ, Radom L, Schleyer PVR, Pople JA (1986) Ab initio molecular orbital theory. Wiley, New York
23. Tomasi J, Persico M (1994) Molecular interactions in solution: an overview of methods based on continuous distributions of the solvent. Chem Rev 94:2027
24. Frisch MJ, Trucks GW, Schlegel HB, Scuseria GE, Robb MA, Cheeseman JR, Scalmani G, Barone V, Mennucci B, Petersson GA, Nakatsuji H, Caricato M, Li X, Hratchian HP, Izmaylov AF, Bloino J, Zheng G, Sonnenberg JL, Hada M, Ehara M, Toyota K, Fukuda R, Hasegawa J, Ishida M, Nakajima T, Honda Y, Kitao O, Nakai H, Vreven T, Montgomery JA, Peralta JE, Ogliaro Jr F, Bearpark M, Heyd JJ, Brothers E, Kudin KN, Staroverov VN, Kobayashi R, Normand J, Raghavachari K, Rendell A, Burant JC, Iyengar SS, Tomasi J, Cossi M, Rega N, Millam JM, Klene M, Knox JE, Cross JB, Bakken V, Adamo C, Jaramillo J, Gomperts R, Stratmann RE, Yazyev O, Austin AJ, Cammi R, Pomelli C, Ochterski JW, Martin RL, Morokuma K, Zakrzewski VG, Voth GA, Salvador P, Dannenberg JJ, Dapprich S, Daniels AD, Farkas O, Foresman JB, Ortiz JV, Cioslowski J, Fox D (2009) Gaussian 09, Revision A.02. Gaussian, Wallingford
25. Reed AE, Curtiss LA, Weinhold F (1988) *Intermolecular interactions from a natural bond orbital, donor-acceptor viewpoint*. Chem Rev 88:899
26. Simkin BY, Sheikhet I (1995) Quantum chemical and statistical theory of solutions—computational approach. Ellis Horwood, London
27. Cances E, Mennucci B, Tomasi J (1997) *A new integral equation formalism for the polarizable continuum model: theoretical background and applications to isotropic and anisotropic dielectrics*. J Chem Phys 107:3032
28. Cossi M, Barone V, Cammi R, Tomasi J (1996) *Ab initio study of solvated molecules: a new implementation of the polarizable continuum model*. Chem Phys Lett 255:327
29. Barone V, Cossi M, Tomasi J (1998) *Geometry optimization of molecular structures in solution by the polarizable continuum model*. J Comput Chem 19:404
30. Becke AD (1993) Density-functional thermochemistry. III. The role of exact exchange. J Chem Phys 98:5648
31. Parr RG, von Szentpaly L, Liu S (1999) *Electrophilicity index*. J Am Chem Soc 121:1922
32. Parr RG, Pearson RG (1983) *Absolute hardness: companion parameter to absolute electronegativity*. J Am Chem Soc 105:7512
33. Parr RG, Yang W (1989) Density functional theory of atoms and molecules. Oxford University Press, New York
34. Domingo LR, Pérez P, Sáez JA (2013) *Understanding the local reactivity in polar organic reactions through electrophilic and nucleophilic Parr functions*. RSC Adv 3:1486
35. Johnson ER, Keinan S, Mori-Sanchez P, Contreras-Garcia J, Cohen J, Yang AW (2010) *Revealing noncovalent interactions*. *J Am Chem Soc* 132:6498
36. Lane JR, Contreras-Garcia J, Piquemal JP, Miller BJ, Kjaergaard HG (2013) *Are bond critical points really critical for hydrogen bonding?* J Chem Theory Comput 9:3263
37. Contreras-Garcia JE, Johnson R, Keinan S, Chaudret R, Piquemal JP, Beratan DN, Yang W (2011) *NCIPLOT: a program for plotting noncovalent interaction regions*. J Chem Theory Comput 7:625
38. Bader RFW (1990) Atoms in molecules. A quantum theory. Claredon Press, Oxford
39. Lu T, Chen F (2012) *Multiwfn: a multifunctional wavefunction analyzer*. J Comput Chem 33:580
40. Domingo LR (2014) A new C–C bond formation model based on the quantum chemical topology of electron density. RSC Adv 4: 32415–32428
41. Reed AE, Weinstock RB, Weinhold F (1985) Natural population analysis. J Chem Phys 83:735–746
42. Becke AD, Edgecombe KE (1990) A simple measure of electron localization in atomic and molecular systems. J Chem Phys 92: 5397–5403
43. Geerlings P, De Proft F, Langenaeker W (2003) Conceptual density functional theory. Chem Rev 103:1793–1873
44. Domingo LR, Ríos-Gutiérrez M, Pérez P (2016) *Applications of the conceptual density functional theory indices to organic chemistry reactivity*. Molecules 21:748
45. Benchouk W, Mekelleche SM, Silvi B, Aurell MJ, Domingo LR (2011) *Understanding the kinetic solvent effects on the 1,3-dipolar cycloaddition of benzonitrile N-oxide: a DFT study*. J Phys Org Chem 24:611
46. Wiberg KB (1968) *Application of the pople-santry-segal CNDO method to the cyclopropylcarbinyl and cyclobutyl cation and to bicyclobutane*. Tetrahedron 24:1083
47. Domingo LR, Aurell MJ, Pérez P, Contreras R (2002) *Quantitative characterization of the global electrophilicity power of common diene/dienophile pairs in Diels-Alder reactions*. Tetrahedron 58: 4417
48. Nacereddine AK, Sobhi C, Djerourou A, Ríos-Gutiérrez M, LR D (2015) *Non-classical CH...O hydrogen-bond determining the regio- and stereoselectivity in the [3 + 2] cycloaddition reaction of (Z)-C-phenyl-Nmethylnitrone with dimethyl 2-benzylidenecyclopropane-1,1-dicarboxylate. A topological electron-density study*. RSC Adv 5:99299
49. Hellel D, Chafaa F, Nacereddine AK, Djerourou A, Vrancken E (2017) *Regio-and stereoselective synthesis of novel isoxazolidine heterocycles by 1, 3-dipolar cycloaddition between C-phenyl-N-methylnitrone and substituted alkenes. Experimental and DFT investigation of selectivity and mechanism*. *RSC Adv* 7:30128–30141
50. Lachtar Z, Nacereddine AK, Djerourou A (2020) *Understanding the origin of the enantioselectivity and the mechanism of the asymmetric reduction of ketimine generated from acetophenone with oxazaborolidine catalyst*. *Struct Chem 31*(1):253–261
51. Chafaa F, Nacereddine AK, Djerourou A (2020) A combined topological ELF, NCI and QTAIM study of mechanism and hydrogen bond controlling the selectivity of the IMDC reaction of nitrone-

alkene obtained from m- allyloxybenzaldehyde. Lett Org Chem 17: 260–267

52. Rozas I, Alkorta I, Elguero J (2000) *Behavior of ylides containing N, O, and C atoms as hydrogen bond acceptors*. J Am Chem Soc 122:11154

53. Grabowski SJ, Sokalski WA, Dyguda E (2006) Leszczynski, J. *Quantitative classification of covalent and non-covalent H-bonds*. J Phys Chem B 110:6444